# Incorporation of Cationic Chains in the Dickerson−Drew Dodecamer: Correlation of Energetics, Structure, and Ion and Water Binding†

Ronald Shikiya,‖ Jian-Sen Li,§ Barry Gold,§,‖,‡,⊥ and Luis A. Marky*,‖,§,‡

*Department of Pharmaceutical Sciences, Department of Biochemistry and Molecular Biology, and Eppley Institute for Research in Cancer, University of Nebraska Medical Center, 986025 Nebraska Medical Center, Omaha, Nebraska 68198-6025*

*Received May 13, 2005*

ABSTRACT: We have investigated the unfolding thermodynamics for incorporating cationic side chains in the Dickerson−Drew dodecamer duplex. Incorporation of two 3-aminopropyl-2′-deoxyuridine residues (one on each self-complementary strand) lowers the stability of the duplex. This reduction is driven by unfavorable heat contributions due to the removal of electrostricted water and higher exposure of polar and nonpolar atomic groups that immobilize structural water. These cationic chains effectively remove counterions from the major groove, neutralizing some negatively charged phosphates. The overall results are consistent with the NMR solution of the modified duplex that showed a small bend at each modified site.

DNA is normally considered a stiff rodlike molecule with a persistent length in excess of 100 base pairs (*1*); however, the binding of proteins can produce significant nonlinear distortions in DNA (*2*, *3*). Several mechanisms have been proposed to account for the distortion induced by DNA binding proteins, and clearly, different proteins can utilize different bending pathways. One feature of some DNA bending proteins is the introduction of cationic side chains, for example, arginine and lysine, into the major groove at the center of the bend or kink. The catabolite activating protein (CAP) transcription factor is an example of this mode of DNA bending. CAP induces a 45° kink in the DNA at the TG step of its TGTGA cognate binding sequence (*4*). These TG steps are well-conserved on both sides of the DNA dyad axis so the CAP dimer bends the DNA by a total angle of 90°. On the basis of the final structure, it is reasonable to assume that the initial binding of CAP to DNA involves hydrogen bonding between Arg and Glu residues of the protein and G and C nucleotides of the TG step at the center of the kinked region. This initial event is followed by salt bridges and additional hydrogen bonds that formed at sequences distal to the bent region. In an effort to understand the effects of basic amino acid side chains in DNA bending as a result of protein binding, we are using 5-(ω-aminoalkyl)-2′-deoxyuridine substitutions to mimic the interactions of the basic amino acids with DNA (*5*, *6*). The location of these cationic side chains was determined to be in the major groove toward the 3′-side using electrostatic footprinting and molecular modeling (*7*, *8*). The NMR solution structure of the modified Dickerson−Drew dodecamer duplex indicates a classical B-DNA structure with normal Watson−Crick base pairing interactions (*9*), confirming the placement and the orientation of the 3-aminopropyl moiety in the major groove toward the 3′-direction from the site of modification. The position of the two charged amino groups resulted in a 0.24-ppm downfield shift of the $^{31}$P resonance located at the phosphodiester linkage between the $^{5'-}$CG$^{-3'}$ steps adjacent to the AT tract. In addition, MD calculations based on the NMR data and electrostatic footprinting (*7*, *8*) predicted that the ammonium group is proximate to the electronegative center at the O$^6$-position of G in this step which requires the modified dodecamer to be bent. The back calculation of NOE data using the bent duplex indicated that the bent structure is consistent with all the available NOE data.

To understand how the positioning of cationic charge in the major groove affects local DNA structure, including their effect on the organization of cations and water, a detailed thermodynamic characterization of DNA containing these modified deoxyuridines is necessary. However, it is equally important to correlate the thermodynamic effects of the incorporation of charged chains with the structural characteristics of similar DNA complexes. For this reason, we have used a combination of optical and calorimetry techniques to investigate the helix−coil transition of the NMR dodecamer duplexes: [d(CGCGAATTCGCG)]$_2$ and [d(CGCGAAT-***N***CGGC)]$_2$, where d***N*** is 5-(ω-aminoalkyl)-2′-deoxyuridine (see Figure 1). We also used UV melting techniques as a function of salt and osmolyte concentration to characterize the counterion and water releases accompanying the unfolding of these duplexes, respectively. The comparison of the resulting thermodynamic profiles yields the specific energetic, ion, and hydration contributions for placing a cationic chain in the major groove of the Dickerson−Drew dodecamer duplex. The results show that the incorporation of the

† This work was supported by Grant CA76049 from the National Institutes of Health, Cancer Center Support Grant CA36727 from the National Cancer Institute, and Grant MCB-0315746 from the National Science Foundation.

* To whom inquires should be addressed. Tel, (402) 559-4628; fax, (402) 559-9543; e-mail, lmarky@unmc.edu.

‖ Department of Pharmaceutical Sciences, University of Nebraska Medical Center.

‡ Department of Biochemistry and Molecular Biology, University of Nebraska Medical Center.

§ Eppley Institute for Research in Cancer, University of Nebraska Medical Center.

⊥ Current address: Department of Pharmaceutical Sciences, University of Pittsburgh, 512 Salk Hall, Pittsburgh, PA 15261.

10.1021/bi050897i CCC: $30.25 
Published on Web 08/24/2005

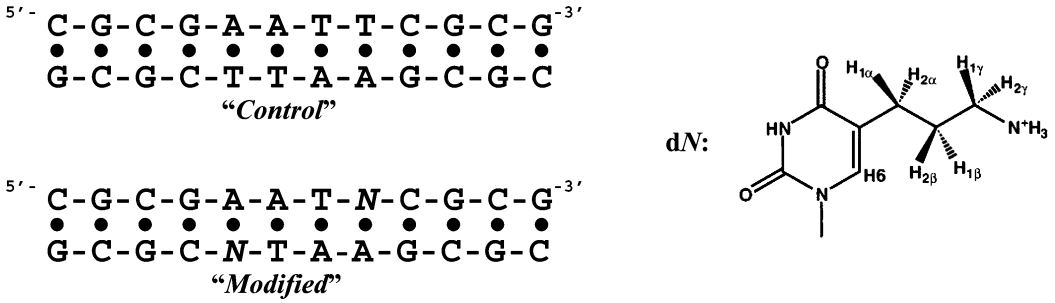


FIGURE 1: The sequence of deoxyribonucleotides and the structure of modified base.

cationic charged chain displaces counterions and water molecules and neutralizes local negative charges, which are consistent with the subtle bend observed at the location of the site of the charged chain in the solution structure of this dodecamer.

## MATERIALS AND METHODS

*Materials.* The phosphoramidite derivative of d*N* was prepared as previously described (*10*, *11*). All oligonucleotides were synthesized in the Eppley Institute Molecular Biology Shared Resource at UNMC, purified by reverse-phase HPLC, desalted on a G-10 Sephadex column, and lyophilized to dryness. The dry oligomers were then dissolved in the appropriate buffer. For simplicity, each duplex is designated as follows: "*Control*", for the unmodified self-complementary dodecamer duplex, $[d(GCCGAATTCGCG)]_2$, and "*Modified*", for the $[d(GCCGAAT\mathbf{\textit{N}}CGCG)]_2$ duplex containing two (one on each strand) 5-(3-aminopropyl)-dU[1] substitutions (Figure 1).

The extinction coefficients of oligonucleotides were calculated in water from the tabulated values of the monomer and dimer nucleotides at 260 nm and 25 °C (*12*). These values were then estimated in the random coil state at 80 °C using a procedure reported earlier (*13*). We obtained a molar extinction coefficient of $1.12 \times 10^5$ $M^{-1}$ $cm^{-1}$ and used this value for both oligonucleotides. The buffer solutions used consisted of 10 mM sodium phosphate at pH 7.0, adjusted to the desired ionic strength with NaCl or desired water activity with ethylene glycol.

*Temperature-Dependent UV Spectroscopy (UV Melting Curves).* Absorption versus temperature profiles (melting curves) for the helix−coil transition of each duplex were obtained with a thermoelectrically controlled UV/Vis Aviv 14DS spectrophotometer, interfaced to a PC computer for data acquisition and analysis. The absorbance at two wavelengths, 260 and 275 nm, were monitored as the temperature was scanned at a heating rate of ∼0.6 °C/min. Analysis of the shape of melting curves yields the transition temperature, $T_M$, and van't Hoff enthalpies, $\Delta H_{vH}$ (*14*). Melting curves as a function of strand were obtained to check the intermolecular formation of each duplex. Additional melting curves were obtained as a function of salt and osmolyte concentration to determine the thermodynamic release of counterions, $\Delta n_{Na^+}$, and the thermodynamic release of water molecules, $\Delta n_W$, respectively, that accompanies their helix → coil transitions.

*Circular Dichroism (CD).* The conformation of each duplex was evaluated by simple inspection of their CD spectrum. The spectrum of each duplex was obtained on an Aviv (model 202SF) circular dichroism spectrometer, using strain-free 1 cm quartz cells, at low temperatures, to ensure 100% duplex formation. The reported spectra correspond to an average of three scans from 320 to 220 nm at a wavelength step of 1 nm.

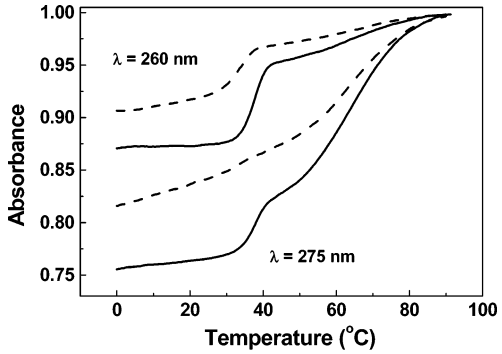


FIGURE 2: UV melting curves of *Control* (solid) and *Modified* dodecamer duplexes (dashed) in 10 mM sodium phosphate buffer at pH 7 at a strand concentration of ∼6 $\mu$M and the wavelengths of 260 and 275 nm.

*Differential Scanning Calorimetry (DSC).* The unfolding heats of each duplex were measured with the VP-DSC differential scanning calorimeter from Microcal, Inc. (Northampton, MA). A typical experiment consists of obtaining a heat capacity profile of a DNA solution against a buffer solution. This experimental curve is normalized by the heating rate, and a buffer versus buffer scan is subtracted using the software of the instrument (Origin V. 5.0). In the case of multiple transitions, this software is able to deconvolute these transitions assuming that the temperature unfolding takes place through sequential independent transitions. The resulting curve for each transition is then integrated, $\int \Delta C_p \, dT$, and normalized for the number of moles, yielding the molar enthalpy, $\Delta H_{cal}$, which is independent of the nature of the transition (*14*). The molar entropy, $\Delta S_{cal}$ is obtained by a similar procedure, $\int (\Delta C_p/T) \, dT$. The free energy at any temperature $T$ is then obtained with the Gibbs equation: $\Delta G°_{cal}(T) = \Delta H_{cal} - T\Delta S_{cal}$, which assumes similar heat capacities for the duplex and random coil states.

## RESULTS

*UV Unfolding of Dodecamer Duplexes.* UV melting experiments at 260 and 275 nm reveal that both duplexes unfold in broad biphasic transitions (Figure 2). At 260 nm, the first transition has a higher hyperchromicity, while at 275 nm the second transition has a larger hyperchromicity. These effects correspond to the unstacking of AT and GC

[1] Abbreviation: dU*, 5-(3-aminopropyl)-2′-deoxyuridine.

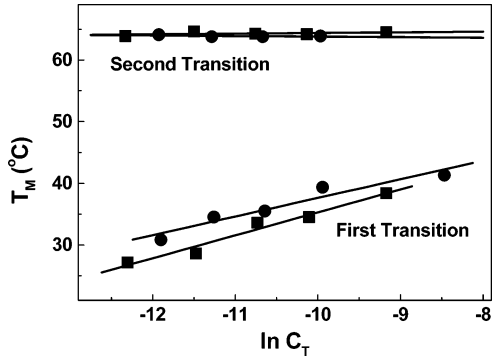


FIGURE 3: $T_M$ dependence on strand concentration for the two transitions of each duplex, *Control* (circles) and *Modified* (squares). The UV melting curves were obtained in 10 mM sodium phosphate buffer at pH 7 using a range of 6−200 $\mu$M (in strands).

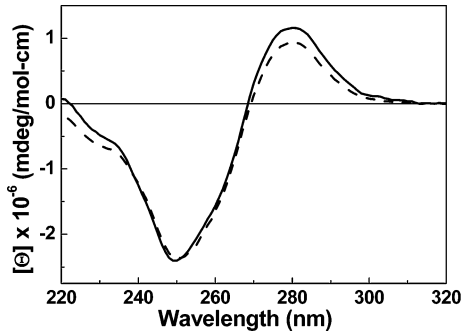


FIGURE 4: CD spectra of the *Control* (solid) and *Modified* (dashed) duplexes in 10 mM sodium phosphate buffer at pH 7 and 5 °C, using a strand concentration of ~6 $\mu$M.

base pairs at 260 nm and the more pronounced unstacking of GC base pairs at 275 nm, respectively. These oligonucleotides are self-complementary and contain complementary CGCG runs at the ends; therefore, the overall melting behavior corresponds to the duplex → hairpin and hairpin → random coil transitions, which is in excellent agreement with earlier unfolding measurements of this dodecamer duplex (*13*). Shape analysis of these melting curves yielded the $T_M$s for each transition. At both wavelengths, the first transition of the *Modified* duplex relative to *Control* has a lower (~3 °C) $T_M$, while the hairpin form of this modified strand has a higher (~2 °C) $T_M$. To confirm the molecularity of each transition, the helix−coil transition of each oligonucleotide was investigated as a function of strand concentration. Melting curves were performed over a 33-fold strand concentration range, and the $T_M$ dependence on strand concentration is shown in Figure 3. The $T_M$s of the first transition increase with strand concentration, while similar $T_M$s are obtained for the second transition. In addition, the $\Delta H_{vH}$ values (80 kcal/mol) for the first transition are much higher than the $\Delta H_{vH}$ values (30 kcal/mol) of the second transition. These results further confirm the sequential duplex → hairpin → single strand melting of each dodecamer duplex.

*CD Spectroscopy.* The CD spectra of each dodecamer duplex at 5 °C are shown in Figure 4. Both duplexes exhibit CD spectra characteristic of a right-handed helix in the "B" conformation. The overlay of the spectra shows similar negative bands, which indicates that both duplexes have similar base-pair stacking interactions; however, the positive bands present some differences in their magnitude, which may be due to small differences in the conformation of the sugar−phosphate backbone. Furthermore, the smaller absolute magnitude of the positive bands, relative to the negative band, suggests the actual contribution of the central core of four AT base pairs. We have not pursued any further analysis of these spectra, other than to show that the duplexes have a B-like conformation with similar base-pair stacking interactions.

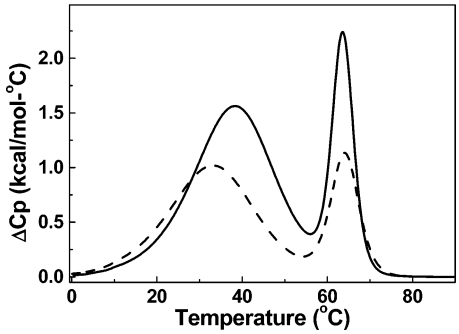


FIGURE 5: DSC melting curves of *Control* (solid) and *Modified* (dashed) duplex in 10 mM sodium phosphate buffer at pH 7 and a total strand concentration of ~200 $\mu$M.

*DSC Unfolding.* Typical excess heat capacity versus temperature profiles (Figure 5) clearly indicate that the helix−coil transitions are biphasic and take place without changes in the heat capacity of the initial and final states. The first transition at low temperatures is broad, while the second transition is sharper at higher temperatures. These thermograms show that each duplex follows a sequential melting of an initial duplex structure to hairpin at low temperatures, and to the final random coil state at higher temperatures, confirming the results of the UV melts. Deconvolution of the two transitions of each dodecamer and integration of each peak yield endothermic enthalpies of 116 kcal/mol (first transition) and 37 kcal/mol (second transition) for the *Control* duplex and much reduced unfolding enthalpies of 68 and 27 kcal/mol for the *Modified* duplex, respectively. The overall heats correspond to the energy needed to disrupt base pairing, base-pair stacking, and the removal of immobilized water molecules, if any.

*Thermodynamic Release of Counterions.* For each duplex, increasing the concentration of $Na^+$ from 16 to 200 mM results in the shift of the melting curves to higher temperatures; that is, the $T_M$ increases (data not shown). The increase in salt concentration shifts the duplex−hairpin−random coil equilibrium toward the conformation with higher charge density parameter (*15*). The $T_M$ dependence on salt concentration for each duplex is shown in Figure 6; linear dependences are obtained with slope values of 7.5 °C (*Control*) and 8.4 °C (*Modified*) for the first transition and much smaller slopes, 3.0 °C (*Control*) and 3.1 °C (*Modified*), for the second transition. The differential ion binding for the helix−coil transition of a molecule, $\Delta n_{Na^+}$, is measured with the relationship (*16*): $\Delta n_{Na^+} = \partial \ln K / \partial \ln (Na^+)$, where $K$ is the equilibrium constant and the $(Na^+)$ term is the ionic activity of $Na^+$, which assumes a similar type of $Na^+$ binding to the helical and coil states. Application of the chain rule yields: $\Delta n_{Na^+} = [\partial \ln K/\partial T_M][\partial T_M/\partial \ln (Na^+)]$, and substituting the van't Hoff equation, $\partial \ln K/\partial T = \Delta H/RT^2$, we obtained: $\Delta n_{Na^+} = 1.1[\Delta H_{cal}/RT_M^2](\partial T_M/\partial \ln [Na^+])$. The 1.1 term is a proportionality constant to convert mean ionic activities into concentrations; the first term in brackets is obtained

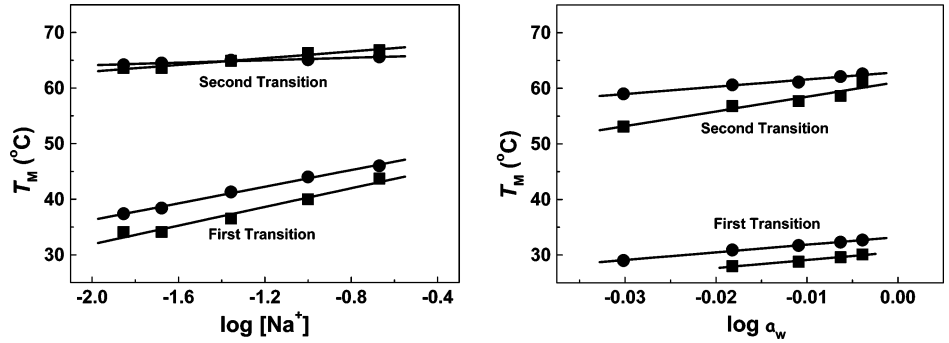


FIGURE 6: The $T_M$ dependences on salt concentration (left panel) and on osmolyte concentration (right panel) are shown for the two transitions of each duplex. The UV melting curves were obtained in 10 mM sodium phosphate buffer at pH 7 and strand concentration of 5 $\mu$M, as a function of salt concentration or ethylene glycol.

directly from DSC experiments, $R$ is the gas constant, while the second term in brackets corresponds to the slope of the lines of Figure 6. We obtained $\Delta n_{Na^+}$ values or counterion releases of 2.3 mol $Na^+$/mol of duplex (*Control*) and 1.5 mol $Na^+$/mol of duplex (*Modified*) for the duplex → random coil transition and a similar release of counterions, 0.2 mol $Na^+$/mol of duplex, for the hairpin → random coil transition of each oligonucleotide.

*Thermodynamic Release of Water.* For each molecule, increasing the concentration of osmolyte (ethylene glycol) from 0.5 to 4 M (i.e., decreasing the activity of water) results in the shift of the melting curves to lower temperatures (data not shown). The increase in water activity shifts the overall equilibrium toward the conformation with higher hydration level, that is, the duplex state. The $T_M$ dependence on water activity for each dodecamer is shown in Figure 6 (right panel). A linear dependence is obtained with slope values in the range of 41 to ~138 °C. The differential water binding for a helix−coil transition, $\Delta n_W$, is measured from the osmotic stress technique using the relationship (*14*): $\Delta n_W = \partial \ln K/\partial \ln (H_2O)$, where $K$ is the equilibrium constant and the ($H_2O$) term is the activity of water, assuming similar type of water binding to both helical and random coil states. Using the chain rule, $\Delta n_W = [\partial \ln K/\partial T_M][\partial T_M/\partial \ln (H_2O)]$, and substituting in the van't Hoff equation, we obtained an equivalent relationship to the differential ion binding (*17*): $\Delta n_W = [\Delta H_{cal}/RT_M^2][\partial T_M/\partial \ln (H_2O)]$. The first term in brackets is obtained from DSC experiments, while the second term in brackets corresponds to the slope of the lines of Figure 6, which is obtained from a plot of the $T_M$ as a function of the concentration of ethylene glycol. The osmolarity of ethylene glycol solutions is measured with a Vapro 5520 vapor pressure osmometer and converted to the activity of water with a calibration curve of NaCl solutions with known activities. We obtained $\Delta n_W$ values, or water releases, of 38 mol $H_2O$/mol duplex (*Control*) and only 7 mol $H_2O$/mol duplex (*Modified*) for the duplex → random coil transition, and similar water releases of 9 mol $H_2O$/mol hairpin (*Control*) and 6 mol $H_2O$/mol hairpin (*Modified*) for the hairpin → random coil transition of each oligonucleotide.

*Standard Thermodynamic Profiles for the Formation of Duplexes.* The free-energy values were calculated at 20 °C from the Gibbs equation, using the enthalpies and entropies obtained in the calorimetric melting experiments: $\Delta G^\circ_{(20)} = \Delta H_{cal} - 293.15\Delta S_{cal}$. In the Gibbs equation, and since we did not find any heat capacity differences between the helical and coil states, both the enthalpy and entropy are considered independent of temperature. Table 1 lists standard thermodynamic profiles for the formation of each duplex molecule at 20 °C, where each parameter is the opposite sign of the unfolding parameter. At this low temperature, the magnitude of the $\Delta G^\circ_{(20)}$ terms indicates that each oligonucleotide forms a stable dodecamer duplex. Dissection of each $\Delta G^\circ_{(20)}$ term shows that the favorable $\Delta G^\circ_{(20)}$ term for the formation of each duplex results from the characteristic partial compensation of a favorable enthalpy and unfavorable entropy terms. The favorable $\Delta H_{cal}$ values is due to the formation of base pairs and base-pair stacks, whereas the unfavorable entropy values indicate contributions from the bimolecular association of two strands to form a duplex, which condenses counterions and immobilizes water molecules, see Table 1.

Table 1: Standard Thermodynamic Profiles for the Formation of Complexes at 20 °C[a]

| duplex | $T_M$ (°C) | $\Delta H_{cal}$ (kcal/mol) | $\Delta G^\circ_{(20)}$ (kcal/mol) | $T\Delta S_{cal}$ (kcal/mol) | $\Delta n_{Na^+}$ (per mol) | $\Delta n_W$ (per mol) |
|---|---|---|---|---|---|---|
| | | | Duplex → Single Strands | | | |
| *Control* | 33.3 | −116 | −6.9 | −109 | −2.3 | −38 |
| *Modified* | 29.8 | −68 | −3.3 | −65 | −1.5 | −7 |
| | | | Hairpin → Single Strands | | | |
| *Control* | 62.8 | −37 | −5.3 | −32 | −0.2 | −9 |
| *Modified* | 64.5 | −27 | −4.0 | −23 | −0.2 | −6 |

[a] All parameters are measured from DSC and UV melting curves in 10 mM sodium phosphate buffer at pH 7.0. The experimental uncertainties are as follow: $T_M$ (±0.5 °C), $\Delta H_{cal}$ (±3%), $\Delta G^\circ_{(20)}$ (±5%), $T\Delta S_{cal}$ (±3%), $\Delta n_{Na^+}$ (±5%) and $\Delta n_W$ (±8%).

## DISCUSSION

*Each Dodecamer Duplex Unfolds through Biphasic Transitions.* Each oligonucleotide forms stable self-complementary duplexes at low temperatures, and their unfolding takes place through sequential biphasic transitions: duplex → hairpin → random coil. This melting behavior is confirmed by the following experimental observations. First, the UV and DSC melting curves unequivocally show two different transitions. Second, their $T_M$s (~31.6 and ~63.7 °C) and hyperchromicity values are consistent with the melting of a dodecamer duplex and a hairpin loop structure with four GC base pairs in the stem, respectively. Third, the $T_M$ of the first transition increases with increased strand concentration and has a strong dependence on salt concentration, while the $T_M$ of the second transition remains the same over a 33-fold change in strand concentration and has only a slight dependence on salt concentration. Fourth, the calorimetric

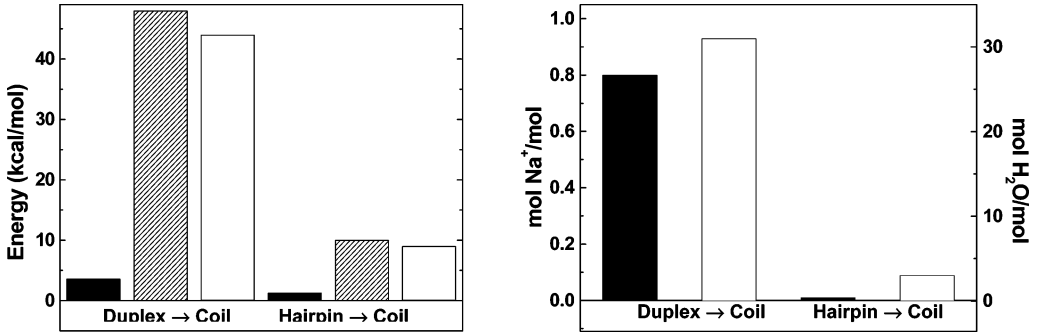


FIGURE 7: Differential thermodynamic profiles for the incorporation of cationic chains to a duplex or hairpin. The left panel correspond to energetics, $\Delta\Delta G°$ (solid bars), $\Delta\Delta H$ (hatch bars), $\Delta(T\Delta S)$ (open bars), while the right panel corresponds to ion and water binding, $\Delta\Delta n_{Na^+}$ (solid bars) and $\Delta\Delta n_W$ (open bars).

and average (*Control* and *Modified*) unfolding enthalpies of ~92 kcal/mol and ~32 kcal/mol in low salt are characteristic of the melting behavior of double helical stems of 12 and 4 base pairs, respectively. This is in good agreement with the predicted enthalpy values of 112 and 36 kcal/mol, obtained from DNA nearest-neighbor parameters for the *Control* duplex (*18*, *19*).

*Thermodynamics of Forming a Duplex and Hairpin with Cationic Chains.* We have investigated two dodecamer duplexes containing specific substitutions at the fifth position of uridine: $-CH_3$ (yielding the normal thymine base) and $-CH_2CH_2CH_2NH_2$. Specifically, we used a combination of UV melting and DSC techniques to determine standard thermodynamic profiles for the unfolding of each self-complementary duplex. Furthermore, the combination of DSC and UV melting techniques allowed us to measure both $\Delta n_{Na^+}$ and $\Delta n_W$ from the model-independent unfolding heats and the $T_M$ dependences on salt and osmolyte concentration (*17*). Complete thermodynamic profiles of duplex formation at 20 °C are shown in Table 1.

For the proper discussion of these profiles, it is important to emphasize the noncovalent interactions that are involved in the favorable formation of a DNA secondary structure, namely, contributions from base pairing, base-pair stacking, and water and counterion binding, which depend on the specific chemical composition of the strands used and overall DNA secondary structure. Table 1 indicates that in low-salt buffer, the favorable formation of each duplex (negative free-energy terms) results from the typical compensation of a favorable enthalpy and unfavorable entropy and the uptake of both ions and water molecules. The resulting exothermic enthalpies correspond to favorable contributions from base pairing, base-pair stacking interactions, uptake of electrostricted water molecules by the base-pair stacks, and the release of structural water from the random coils prior to forming duplexes. The uptake of counterions is considered to have a negligible heat contribution (*20*), while the unfavorable entropy terms correspond to contributions of forming a higher-ordered duplex structure resulting from the bimolecular association of two strands, and the overall condensation of counterions and immobilization of water molecules.

*Thermodynamic Impact for the Incorporation of a Cationic Chain into DNA.* The thermodynamic contributions for the incorporation of two cationic chains into a DNA duplex are best-illustrated using a thermodynamic cycle in which the formation of the unmodified duplex is used as the reference reaction. The difference between these two strands is a charged aminoethyl group; however, we assumed that their random coils behave similarly at temperatures well above the $T_M$ with respect to base stacking interactions and ion and water binding. Relative to the unmodified dodecamer, and using the first set of thermodynamic profiles (Table 1) that correspond to the transition of a duplex to the random coil state, we obtained an unfavorable $\Delta\Delta G°$ of 3.6 kcal/mol resulting from a large compensation of an unfavorable $\Delta\Delta H_{cal}$ of 48 kcal/mol with a favorable $\Delta(T\Delta S_{cal})$ term of 44 kcal/mol (Figure 7, left panel). The differential enthalpy term indicates differences in base stacking and hydration between the two duplexes, while the differential entropy term is consistent with both a net counterion release of 0.8 mol $Na^+$/mol duplex and a water release of 31 mol water/mol duplex (Figure 7, right panel). The overall effects are consistent with the presence of the tethered amino charge that directly or indirectly neutralizes charge on the phosphate backbone, and perhaps allows some changes in the exposure of aromatic bases to the solvent. Similarly, to determine the thermodynamic contributions for the inclusion of a single cationic chain in the loop of this dodecamer, we use the thermodynamic parameters for the unfolding of the hairpins to the random coil state (second set of Table 1), and by setting up a similar thermodynamic cycle relative to the unmodified hairpin, we obtained an unfavorable $\Delta\Delta G°$ of 1.3 kcal/mol resulting from the compensation of an unfavorable $\Delta\Delta H_{cal}$ of 10 kcal/mol with a favorable $\Delta(T\Delta S_{cal})$ term of 9 kcal/mol (Figure 7, left panel). The $\Delta\Delta H_{cal}$ term indicates both differences in base-stacking contributions, if any, and overall hydration within the constrained loops of the two hairpins, while the $\Delta(T\Delta S_{cal})$ term is consistent with an additional ordering of the modified constrained loop and a small net water release of 3 mol water/mol hairpin. The incorporation of the cationic chain in the loop does not release any additional counterions (Figure 7, right panel). This latter set of differential thermodynamic profiles can be used as an internal control for the interpretation of the thermodynamic data of the placement of a single cationic chain in the dodecamer duplex. As expected, the placement of a single cationic chain in the loop, and relative to the placement of a single chain in the duplex, yielded much lower differential thermodynamic contributions: $\Delta\Delta G° = 0.5$ kcal/mol, $\Delta\Delta H = 14$ kcal/mol and $\Delta(T\Delta S) = 13$ kcal/mol. These parameters correspond to additional short- and long-range thermodynamic effects for the placement of cationic charge in a DNA duplex.

*Incorporation of the Cationic Chain Releases Electrostricted Water and Immobilizes Structural Water Molecules.* To answer the question of how cationic charge can affect DNA structure, we inspect the differential thermodynamic profiles of the duplex → coil transition. The resulting differential profile is shown in Figure 7 (left panels). The incorporation of a single cationic charge causes a destabilization of the dodecamer duplex, $\Delta\Delta G^\circ = 1.8$ kcal/mol, which is in disagreement to what has been observed earlier in similar incorporations at comparable salt concentrations. To explain this counterintuitive destabilizing effect, we invoke hydration differences of the neighboring base sequences of the modified base (*21*, *22*) (T***N***CG vs G***N***CG); that is, the aminopropyl-2′-deoxyuridine is at the junction of a well-hydrated four AT bases pairs and the CG base pair ends (*20*). The induced destabilization is enthalpy-driven ($\Delta\Delta H = 24$ kcal/mol), indicating a putative reduction in base-pair stacking contributions and lower hydration levels in the modified duplex. Decreased binding of counterions does not appear to contribute at all. However, the similarity of the CD spectra shows that both duplexes have comparable base-pair stacking interactions, consistent with the NMR data that show intact base pairs (*9*). This suggests that the differential heat contribution is mainly due to a lower hydration level of the modified duplex, which correlates with the measured differential hydration of 31 water molecules. Furthermore, the differential thermodynamic profiles for the incorporation of the cationic chain in the loop also indicate that the modified hairpin is less stable ($\Delta\Delta G^\circ = 1.3$ kcal/mol) due to unfavorable heat contributions ($\Delta\Delta H = 10$ kcal/mol). This also points toward a lower hydration level of the modified loop; hence, the cationic chain induces small changes in the stacking of bases with higher exposure of the constrained bases of this loop to the solvent. The favorable $\Delta(T\Delta S_{cal})$ term is consistent with the exclusion of both counterions and water molecules from the duplex, suggesting that the presence of the cationic chain in the major groove causes a rearrangement of the overall counterion−water ionic atmosphere of the duplex.

We have developed a physical signature for determining the types of water, electrostricted (around charged groups) versus structural (around polar and nonpolar groups), that are involved in a particular thermodynamic process. This consists of the comparison of the signs of the differential energy (or differential enthalpy−entropy compensation) with the differential volume change: similar signs of these parameters indicate the involvement of electrostricted water, while opposite signs indicate structural water; that is, energy is needed for both removal of electrostricted water and immobilization of structural water (*23*, *24*). The measured release of water molecules for the placement of a cationic chain in the major groove corresponds to a positive differential change in volume, which is of similar sign with a positive differential free energy and with a positive differential enthalpy−entropy compensation, and shows a net displacement of electrostricted water molecules. However, the release of 15.5 mol of electrostricted water per cationic chain, and using a heat of 0.3 mol kcal/mol for the removal of this type of water (*25*), contributes an enthalpy term of ∼5 kcal. This is smaller than the measured $\Delta\Delta H$ of 24 kcal/mol of cationic chain. Where does the difference of 19 kcal come from? One possibility is a higher exposure of polar and nonpolar groups to the solvent, which is due to a DNA deformation induced by the presence of the cationic side chain that generates a small, local, helical bend. This interpretation is consistent with the NMR studies of this structure (*9*). The higher exposure of surface area by the bent duplex immobilizes structural water, which may contribute with the additional endothermic heat.

To understand how the aminopropyl-induced bending of the DNA would affect the hydrophobic surface exposed to solvent, the SASA of the NMR structures (linear and bent) were determined (*22*). The surface areas for the bent (constrained) and linear (unconstrained) NMR structures were 3631 and 3587 Å$^2$, respectively. This calculates to an increase of 25 Å$^2$ per modified residue. The same type of surface analysis was done using the same DNA structures except the aminopropyl chain was replaced by a hydrogen atom to eliminate any effect due to the location of the side chain in the major groove. In this case, the bent structure has approximately 33 Å$^2$ more surface area per modified residue than the linear structure. Therefore, the bent structure from NMR is consistent with the conclusion from the thermodynamic studies that the modified DNA is exposing more polar and nonpolar surface to the solvent.

For the interpretation of the lower water uptake by the modified duplex, we suggest that the osmotic stress technique measures the number of water molecules that are tightly associated with DNA. This type of water could very well be the electrostricted water that is associated with the negative phosphate groups of DNA. Alternatively, melting experiments are performed by changing the temperature, and these temperature changes may gradually release structural water that is immobilized around polar and nonpolar groups of the exposed aromatic bases.

*The Incorporation of Cationic Chains Displaces Counterions from the Major Groove.* The placement of cationic chains reduces the uptake of counterions by the dodecamer duplex, while no effect is observed with the two hairpins. This shows that the positively charged aminopropyl side chain at pH 7 is partially neutralizing the negative charges in the dodecamer duplex. The actual degree of neutralization of negative phosphate charge by the cationic charge may be estimated from the 0.8 mol $Na^+$/mol hairpin differential uptake of counterions. A ∼15% higher phosphate neutralization is estimated for the local placement of the aminopropyl chain in the major groove of the CG/GC base-pair stack adjacent to the AT tract of the modified duplex, which is in excellent agreement with the 14% charge neutralization in a similar base-pair stack environment of a hairpin stem (*21*), and consistent with the 0.24-ppm downfield shift of the $^{31}P$ resonance located in this base-pair step. We stress that the aminopropyl group does not form a salt bridge with the phosphate backbone (*7*, *8*, *26*) but rather causes a reorganization of the groove counterions around the tethered amine group; that is, neutralization of charge may be indirect. This indirect charge neutralization could occur by the proposed electrostatic mechanism of Rouzina and Bloomfield (*27*). In this mechanism, the local presence of the cationic aminopropyl chain (rather than divalent cations used in the calculations of Rouzina and Bloomfield) located in the major groove of DNA repels $Na^+$ counterions yielding unscreened phosphates that are more attracted to the propyl-tethered cation chain. This scenario is consistent with our thermo-

dynamic results and nicely explains how the incorporation of $\omega$-aminoalkyl side chains induce DNA bending.

## CONCLUSIONS

In this work, we focused on the overall thermodynamics of unfolding of the Dickerson−Drew dodecamer structure that is distorted by the inclusion of tethered cations. We were able to shed light on specific contributions to DNA bending by setting up appropriate thermodynamic cycles, that is, using the unmodified duplex as a control. UV and DSC melting protocols were used to investigate the helix−coil transitions of a pair of DNA duplexes with and without the cationic chains. The temperature-induced unfolding of each duplex takes place through the sequential melting of a duplex → hairpin → random coil. The $T_M$ of each transition increases with an increase in salt concentration and decreases with a decrease in the activity of water. The differential thermodynamic profile pertaining to the incorporation of two aminopropyl chains in the major groove of the dodecamer duplex is $\Delta\Delta G^\circ = 3.6$ kcal/mol, $\Delta\Delta H = 48$ kcal/mol, $\Delta\Delta S = 150$ cal/(K mol), $n_{Na}{}^+ = 0.8$ mol $Na^+$/mol, and $\Delta\Delta n_W = 31$ mol $H_2O$/mol. Thus, the placement of cationic chains yields a duplex with lower stability primarily because of unfavorable heat contributions that are due to the removal of electrostricted water and immobilization of structural water by the higher exposure of polar and nonpolar atomic groups to solvent. Furthermore, the location of these chains effectively and regiospecifically removes counterions from the major groove, directly or indirectly neutralizing negatively charged phosphates. The overall results are consistent with, and provide a mechanistic explanation of, the NMR solution structure of the modified self-complemenary dodecamer duplex that showed a small bend at each modified site.

## REFERENCES


1. Hagerman, P. J. (1988) Flexibility of DNA, *Annu. Rev. Biophys. Biophys. Chem. 17*, 265−286.
2. Young, M. A., Ravishanker, G., Beveridge, D. L., and Berman, H. M. (1995) Analysis of local helix bending in crystal structures of DNA oligonucleotides and DNA−protein complexes, *Biophys J. 68*, 2454−2468.
3. Luger, K., Mader, A. W., Richmond, R. K., Sargent, D. F., and Richmond, T. J. (1997) Crystal structure of the nucleosome core particle at 2.8 Å resolution, *Nature 389*, 251−260.
4. Schultz, S. C., Shields, G. C., and Steitz, T. A. (1991) Crystal structure of a CAP−DNA complex: the DNA is bent by 90 degrees, *Science 253*, 1001−1007.
5. Strauss, J. K., Roberts, C., Nelson, M. G., Switzer, C., and Maher, L. J., III (1996) DNA bending by hexamethylene-tethered ammonium ions, *Proc. Natl. Acad. Sci. U.S.A. 93*, 9515−9520.
6. Strauss, J. K., Prakash, T. P., Roberts, C., Switzer, C., and Maher, L. J., III (1996) DNA bending by a phantom protein, *Chem. Biol. 3*, 671−678.
7. Liang, G., Encell, L., Nelson, M. G., Switzer, C., Shuker, D. E. G., and Gold, B. (1995) Role of electrostatics in the sequence-selective reaction of charged alkylating agents with DNA, *J. Am. Chem. Soc. 117*, 10135−10136.
8. Dande, P., Liang, G., Chen, F.-X., Roberts, C., Nelson, M. G., Hashimoto, H., Switzer, C., and Gold, B. (1997) Regioselective effect of zwitterionic DNA substitutions on DNA alkylation: evidence for a strong side chain orientational preference, *Biochemistry 36*, 6024−6032.
9. Li, Z., Huang, L., Dande, P., Gold, B., and Stone, M. P. (2002) Structure of a tethered cationic 3-aminopropyl chain incorporated into an oligodeoxynucleotide: evidence for 3′-orientation in the major groove accompanied by DNA bending, *J. Am. Chem. Soc. 124*, 8553−8560.
10. Hashimoto, H., Nelson, M. G., and Switzer, C. (1993) Zwitterionic DNA, *J. Am. Chem. Soc. 115*, 7128−7134.
11. Hashimoto, H., Nelson, M. G., and Switzer, C. (1993) Formation of chimeric duplexes between zwitterionic and natural DNA, *J. Org. Chem. 58*, 4194−4195.
12. Cantor, C. R., Warshow, M. M., and Shapiro, H. (1970) Oligonucleotide interactions. 3. Circular dichroism studies of the conformation of deoxyoligonucleotides, *Biopolymers 9*, 1059−1077.
13. Marky, L. A., Blumenfeld, K. S., Kozlowski, S., and Breslauer, K. J. (1983) Salt-dependent conformational transitions in the self-complementary deoxydodecanucleotide d(CGCGAATTCGCG): evidence for hairpin formation, *Biopolymers 22*, 1247−1257.
14. Marky, L. A., and Breslauer, K. J. (1987) Calculating thermodynamic data for transitions of any molecularity from equilibrium melting curves, *Biopolymers 26*, 1601−1620.
15. Manning, G. Q. (1978) The molecular theory of polyelectrolyte solutions with applications to the electrostatic properties of polynucleotides, *Rev. Biophys. 11*, 179−246.
16. Cantor, C. R., and Schimmel, P. R. (1980) *Biophysical Chemistry*, W. H. Freeman and Company, New York.
17. Spink, C. H., and Chaires, J. B. (1999) Effects of hydration, ion release, and excluded volume on the melting of triplex and duplex DNA, *Biochemistry 38*, 496−508.
18. Breslauer, K. J., Frank, R., Blocker, H., and Marky, L. A. (1986) Predicting DNA duplex stability from the base sequence, *Proc. Natl. Acad. Sci. U.S.A. 83*, 3746−3750.
19. SantaLucia, J., Jr. (1998) A unified view of polymer, dumbbell and oligonucleotide DNA nearest-neighbor thermodynamics, *Proc. Natl. Acad. Sci. U.S.A. 95*, 1460−1465.
20. Marky, L. A., and Kupke, D. W. (1989) Probing the hydration of the minor groove of A·T synthetic DNA polymers by volume and heat changes, *Biochemistry 28*, 9982−9988.
21. Soto, A. M., Kankia, B., Dande, P., Gold, B., and Marky, L. A. (2001) Incorporation of a cationic aminopropyl chain in DNA hairpins: thermodynamics and hydration, *Nucleic Acids Res. 29*, 3638−3645.
22. Soto, A. M., Kankia, B., Dande, P., Gold, B., and Marky, L. A. (2002) Thermodynamic and hydration effects for the incorporation of a cationic 3-aminopropyl chain into DNA, *Nucleic Acids Res. 30*, 3171−3180.
23. Marky, L. A., and Kupke, D. W. (2000), Enthalpy−entropy compensations in nucleic acids: contribution of electrostriction and structural hydration, *Methods Enzymol. 323*, 419−441.
24. Marky, L. A., Rentzeperis, D., Luneva, N. P., Cosman, M., Geacintov, N. E., and Kupke, D. W. (1996) Differential hydration thermodynamics of stereoisomeric DNA−benzo[*a*]pyrene adducts derived from diol epoxide enantiomers with different tumorigenic potentials, *J. Am. Chem. Soc. 118*, 3804−3810.
25. Gasan, A. J., Maleev, V. Y., and Semenov, M. A. (1990) Role of water in stabilizing the helical biomacromolecules DNA and collagen, *Stud. Biophys. 136*, 171−178.
26. Heystek, L. E., Zhou, H.-Q., Dande, P., and Gold, B. (1998) Control over the localization of positive charge in DNA: the effect on duplex DNA and RNA stability, *J. Am. Chem. Soc. 120*, 12165−12166.
27. Rouzina, I., and Bloomfield, V. A. (1998) DNA bending by small, mobile multivalent cations, *Biophys. J. 74*, 3152−3164.


BI050897I